ADVANCED ENERGY & SUSTAINABILITY RESEARCH
Open Access
www.advenergysustres.com

Direct Cation Stabilization Effects of CO Dimerization for Boosting C_2 Pathways of CO_2 Reduction on Noble Metal Surfaces

*Hon Ho Wong, Mingzi Sun, Tong Wu, Lu Lu, Qiuyang Lu, Baian Chen, Cheuk Hei Chan, and Bolong Huang**

The carbon dioxide reduction reaction (CO_2RR) is one of the most promising solutions for realizing carbon neutralization via converting the emitted CO_2 into value-added chemicals. The C—C coupling step for CO dimerization is the rate-determining step for C_2 pathways, which have not been thoroughly investigated. Herein, the direct cation stabilization effects on CO dimerization for *OCCO formation on the representative Cu(100) and Pt(100) surfaces are investigated. Density functional theory calculations show that the presence of alkali metal ions plays a vital role in promoting the coupling of *CO monomers on both metal surfaces, where Cu shows a stronger stabilization effect. More importantly, a strong linear correlation ($R^2 \approx 0.9$) between the dimer stabilization energy and the reaction energy is revealed for the first time, which is a promising indicator for the selectivity of C_2 pathways. Further investigations on electronic structures reveal that the promoting effect on *OCCO formation is strongly related to the negative charges of the molecules, in which the negative charge accumulation is favored by the directional electron transfer due to the chemisorption of *OCCO on Cu(100) surface. This work offers insights into the understanding of C—C coupling reactions for CO_2RR mechanisms.

1. Introduction

Carbon dioxide (CO_2) accumulation in the atmosphere has contributed to the greenhouse effect, leading to dangerous climate changes worldwide. The research community has been seeking an alternative clean energy source to reduce carbon emissions from burning fossil fuels. Carbon dioxide reduction reaction (CO_2RR) was one of the most crucial carbon conversion techniques to realize renewable energy storage and carbon neutralization.[1] The CO_2RR is regarded as the reversed process of fossil fuel combustion, which transforms the CO_2 molecule into various valuable hydrocarbons and alcohol substances, such as methane, ethylene, and ethanol. Unfortunately, CO_2 possesses high chemical stability owing to its high bonding energy of C═O bonds (750 kJ mol^{-1}), which is considerably higher than C—C (336 kJ mol^{-1}), C—O (327 kJ mol^{-1}), and C—H (411 kJ mol^{-1}), making the conversion of CO_2 into other chemical is a considerable challenge.[2] Both experimental and theoretical studies on CO_2RR have realized satisfactory progress toward the C_1 product pathways.[3] Unfortunately, the complex mechanism hindered the investigation of the C_2 product pathways. Generating C_2 products on metal catalyst surfaces is typically difficult to control, and only limited metal surfaces, such as copper (Cu) surfaces, can realize C_2 product formation.[4]

Different from C_1 products, generating C_2 products involves complex reduction pathways with numerous reaction intermediates. The critical step toward the C_2 product formation on the metal surface is the C—C coupling between two C_1 intermediates, in which the dimerization between carbon monoxide (CO) intermediates is the rate-determining step of the C_2 pathways.[5] Although the CO dimer, also known as ethylene dione (OCCO), is the key intermediate for forming C_2 products, it is a precarious molecule that tends to dissociate into two CO molecules readily.[6] Theoretical studies have indicated that the energy barrier for CO dimerization on metal surfaces is excessively high to overcome, and the reaction energies of *OCCO formation are also highly endergonic under vacuum.[5a] Meanwhile, the presence of cations, such as potassium ions (K^+), lithium ions (Li^+), and cesium ions (Cs^+), has played a significant role during the CO coupling process by introducing the cation effects.[7] The cation effects facilitate the formation of *OCCO on metal electrodes, which strongly correlate with the size and solvation energy of the cation. One of the possible

H. H. Wong, M. Sun, T. Wu, L. Lu, Q. Lu, B. Chen, C. Hei Chan, B. Huang
Department of Applied Biology and Chemical Technology
The Hong Kong Polytechnic University
Hung Hom, Kowloon, Hong Kong SAR 999077, China
E-mail: bhuang@polyu.edu.hk

B. Huang
Research Centre for Carbon-Strategic Catalysis (RC-CSC)
The Hong Kong Polytechnic University
Hung Hom, Kowloon, Hong Kong SAR 999077, China

The ORCID identification number(s) for the author(s) of this article can be found under https://doi.org/10.1002/aesr.202400110.

DOI: 10.1002/aesr.202400110

explanations is that the solvated cations in the outer Helmholtz plane (OHP) induce a modification in the surface charge density and boost CO dimerization.[8] Recent studies have also shown that forming hydrogen bonds between the H_2O and intermediate is critical for stabilizing the *OCCO on the metal surface.[9] At the same time, the presence of cations influences this solvation effect and affects CO dimerization.[10] In addition, Koper et al.[11] found that the effects of cations on the C_2 product selectivity are potential- dependent. However, most previous studies only emphasize the solvation effects induced by water molecules while the intrinsic effects caused by cations have rarely been discussed.

In this work, we have conducted density functional theory (DFT) calculations of the direct cation effects in the CO dimerization process on the Cu(100) surface (Figure S1–S4, Supporting Information) and Pt(100) surface (Figure S5–S8, Supporting Information). From the thermodynamic perspective, the direct stabilization effects of common alkali ions, such as Li^+, K^+, Na^+, and Cs^+, on the CO dimerization have been evaluated. We have revealed a strong correlation between the direct stabilization energy induced by the cation with both the reaction energy and the activation barrier of the CO dimerization process. In addition, we explored the modification of electronic structure by introducing alkali ions via Mulliken charge and density of states (DOS) analysis, which explains the origins of the cation effect for promoting CO_2RR performances. This work has offered significant references for understanding the cation effect in CO_2RR, which facilitates the improvement of C_2 selectivity in future research.

2. Results and Discussions

2.1. *OCCO Adsorption with the Presence of Cations

Two binding configurations are adopted for the *OCCO adsorption on the metal surface. Literature commonly reported that *OCCO binds on the surface via both C atoms (C—C binding mode). In some cases, it is also possible to bind the *OCCO via one side of the O—C placed parallel to the surface while another side of the molecule lifts from the surface (O—C binding mode). However, DFT calculations showed that the O—C binding mode is the only stable adsorption configuration on the Cu(100) surface in the vacuum–metal interface.[5a] Our DFT calculation supports the previous studies that the C—C binding mode of *OCCO becomes feasible by adding cation species into the vacuum layer. Interestingly, the C—C binding mode and O—C binding mode of *OCCO were found on the Pt(100) even without charged species due to the strong *OCCO adsorption, but our further investigation revealed that the strong binding is not necessarily beneficial to the C—C coupling. Our work employed the more commonly reported C—C binding mode for further calculation and discussion.

The optimized *OCCO on Cu(100) and Pt(100) surfaces showed varying bond lengths and adsorption strength depending on the added cationic species. In **Table 1**, ΔE_{OCCO}, ΔE_{2CO}, and ΔE_{cation} represent the adsorption energy (ΔE_{ads}) of *OCCO, *CO, and cation, respectively. At the same time, the d_{C-C}, d_{C-O}, and d_{C-M} are the C—C bond length, C—O bond length, and the distance between the C atom and the metal surface, respectively. As shown in Table 1, changing the alkali metal ion leads to a variation in d_{C-C}. Especially on the Cu(100) surface, a significant C—C bond length variation was observed. Across the alkali metal ions, the d_{C-C} decreased from 1.610 to 1.482 Å by changing the cation from Cs^+ (167 pm) to Li^+ (90 pm), suggesting that a strong C—C bonding form with a smaller alkali metal cation. On the other hand, our calculations also found a C—O bond stretching. Compared with two individual *CO molecules binding on the T-sites, the d_{C-O} elongated from 1.170 to over 1.240 Å on Cu(100) and Pt(100) surfaces after the *OCCO formation, which resulted from the intramolecular repulsion between the lone pair electron on O atom. It is also noticed that the *OCCO with larger alkali metal ions has less C—O bond elongation. Since the exothermic C—C bond formation also serves as the primary thermodynamic driving force for the CO dimerization process, a portion of the energy released from this bonding compensates for the energy cost of the C—O bond stretching during coupling. Although the values of d_{C-M} between *OCCO and metal surface are similar on Cu(100) and Pt(100), the adsorption strength of *OCCO on Pt(100) surface was much stronger than that on Cu(100) surface, indicating over binding of *OCCO on Pt(100) surface. Literature pointed out that such strong adsorption of the intermediate may contribute to the poor performance of CO_2RR of Pt-surface.[12]

On the other hand, the larger alkali metal ion significantly strengthens the *OCCO adsorption on both Cu(100) and Pt(100) surfaces. The ΔE_{OCCO} decreased from −0.87 to −1.43 eV and −2.97 to −3.18 eV when changing the cation from Li^+ to Cs^+ on Cu(100) and Pt(100) surface, respectively. However, the adsorption energy variation for the Pt(100) surface was relatively

Table 1. Bond length of the *OCCO under different alkali metal ions and the corresponding adsorption energy.

Surface	Cation	d_{C-C} [Å]	d_{C-O} [Å]	d_{C-M} [Å]	ΔE_{OCCO} [eV]	ΔE_{2CO} [eV]	ΔE_{cation} [eV]
Cu (100)	Li^+	1.482	1.300	1.928	−0.87	−1.43	−7.19
	Na^+	1.562	1.261	1.935	−1.24	−1.57	−6.86
	K^+	1.571	1.257	1.945	−1.31	−1.58	−6.38
	Cs^+	1.610	1.242	1.946	−1.43	−1.59	−6.11
Pt (100)	Li^+	1.519	1.266	1.964	−2.97	−3.23	−1.39
	Na^+	1.539	1.254	1.967	−3.06	−3.33	−0.88
	K^+	1.557	1.243	1.976	−3.16	−3.34	−0.47
	Cs^+	1.573	1.238	1.975	−3.18	−3.24	−0.20

minor compared to that of the Cu(100) surface, revealing that the strong *OCCO binding on Pt(100) was less affected by the surrounding cations. This strengthening of *OCCO adsorption is attributed to the electronic modification of the metal surface, in which the alkali metal ions with larger ionic radii imposed a more significant influence on the surface electronic structure. In addition, the adsorption strengths of the initial 2* CO and the final *OCCO products were compared, and the difference between ΔE_{2CO} and ΔE_{OCCO} can be used to demonstrate the weakening of the C—M interaction with the stronger C—C bonding (shorter the C—C bond length). As shown in Table 1, the adsorption energy *OCCO is much less negative than the adsorption energy of initial 2* CO, which suggests that the formation of the C—C bond weakens the carbon–metal (C—M) interaction on Cu(100) and Pt(100) surfaces. Moreover, **Figure 1** also demonstrates that the weakening of the C—M interaction was proportional to the C—C bond length of the *OCCO, in which the stronger C—C bonding (shorter the C—C bond length) on the adsorbed *OCCO show more weakening on the C—M interaction after the *OCCO formation. For the adsorption strength of cation species on metal surfaces, the cations were strongly binding on Cu(100) surfaces with $\Delta E_{cation} < -6.00$ eV, especially the smaller cations (Li^+ and Na^+) have stronger binding than the larger cations (K^+ and Cs^+). For the Pt(100) surface, the trend of ΔE_{cation} did not change when varying the cation, the binding of cations was significantly weaker when compared with the Cu(100) surface. Overall, the adsorption energy calculation showed an opposite trend of the ΔE_{OCCO} and ΔE_{cation} on Cu(100) and Pt(100) surfaces, in which the Cu(100) tends to bind cations strongly but weakly bind *OCCO, while the Pt(100) surface over-bind *OCCO but adsorbed cations weakly. Notably, the strong cation on the Cu(100) surface may also lead to a steric effect during the electrochemical processes. A previous study demonstrated that cation adsorption on Cu-based material could accelerate the CO dimerization reaction via steric effect.[13]

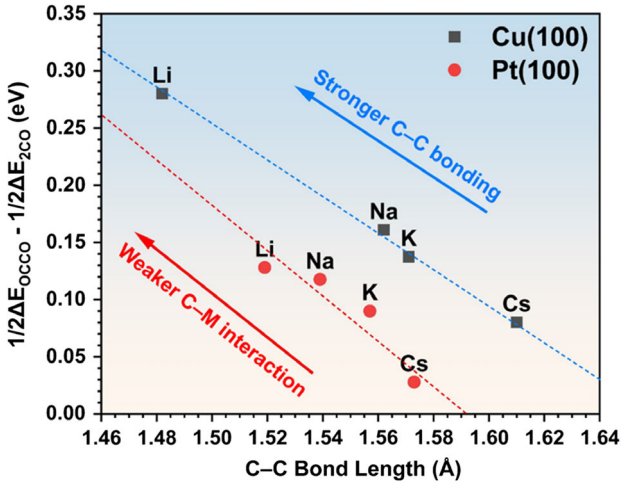

Figure 1. The change of the adsorption energy difference between *OCCO and *CO on Cu(100) and Pt(100) against the C—C bond length variation of the formed *OCCO.

2.2. Reaction Energy and Activation Barrier of CO Dimerization

To assess the thermodynamic feasibility of the CO dimerization on Cu(100) and Pt(100) surfaces with the direct cation effect of the alkali metal ions, the reaction energy (ΔH_{OCCO}) of the *OCCO formation has been calculated. The reaction energy (ΔH_{OCCO}) represents the energy difference between the final product (*OCCO) and initial reactants (2*CO). Table 1 shows that the d_{C-C} and d_{C-O} of final state (FS) *OCCO vary under the presence of different cations, which made the FS different in energies with various cations (**Figure 2**). The FS of the CO dimerization was defined as the most stable *OCCO on the Cu(100) and Pt(100) surfaces after the DFT geometry optimization. The convergence criteria of DFT geometry optimization for the determination of FS were shown in the Method section. Even with alkali metal ions, the DFT calculation predicted a relatively

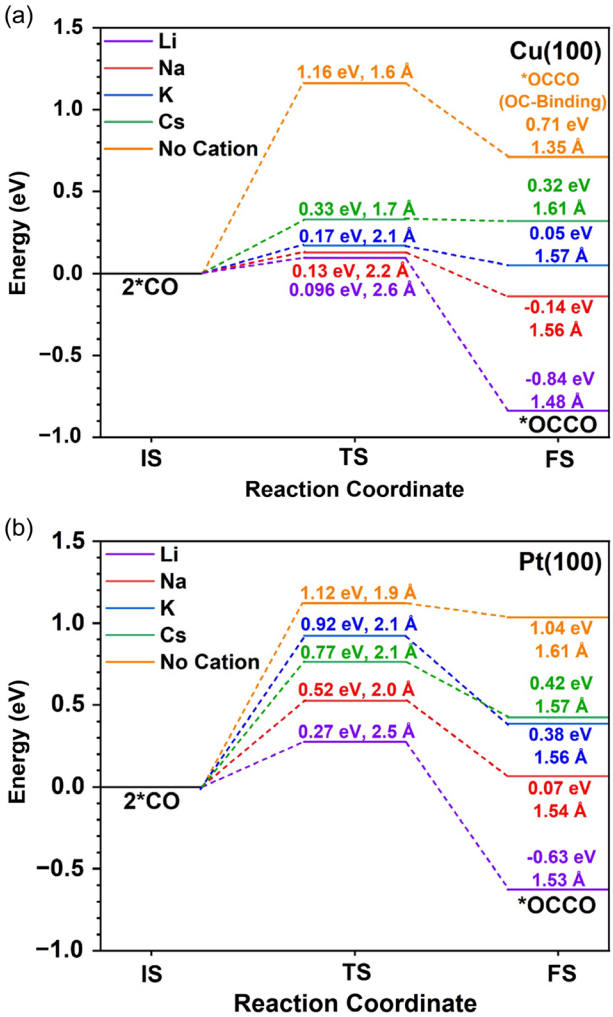

Figure 2. The reaction energy diagram of reaction paths for the CO dimerization on a) Cu(100) surface and b) Pt(100) surface. The energies and bond length shown above the transition state (TS) are the energy barrier and corresponding d_{C-C} at TS. The energies and bond length shown on the final state (FS) are the reaction energy for *OCCO formation and corresponding d_{C-C} at FS. All energies are relative to the energy of the co-adsorbed 2*CO initial state (IS) on two neighboring T-sites.

poor thermal feasibility of *OCCO formation on Pt(100). Without the presence of cations, the formation of *OCCO dimer required a very high ΔH_{OCCO} of 1.04 eV for Pt(100) surface. The ΔH_{OCCO} reduces significantly with the presence of alkali metal ions. The formation of *OCCO remained endergonic on the Pt(100) surface with Na^+, K^+, and Cs^+ (0.07, 0.38, and 0.42 eV, respectively). Only the smallest alkali metal ion, Li^+, has the exergonic CO dimerization with ΔH_{OCCO} of −0.63 eV.

On the other hand, the *OCCO formation was relatively more thermodynamically favorable on the Cu(100) surface with the cation effect according to the negative ΔH_{OCCO}. As mentioned earlier, only the O—C binding mode was found on the Cu(100) surface with high ΔH_{OCCO} of 0.71 eV when no charged species are present. In contrast, the coupling process became exergonic under the influence of smaller cations Li^+ and Na^+ ($\Delta H_{OCCO} = -0.86$ and −0.15 eV, respectively) and showing a near-zero ΔH_{OCCO} for K^+. Notably, the Cs^+ showed endergonic coupling processes with ΔH_{OCCO} of 0.32 eV. These results confirm that the size of alkali metal cations influences the reaction energy for CO dimerization, in which the smaller cations are more effective in facilitating the *OCCO formation. Interestingly, the previous studies showed a reverse trend when accounting for the solvation environment, where larger cations enhanced CO dimerization more effectively on metal surfaces. In contrast, the effect of smaller cations was blocked due to the strong water solvation.[9,14] Our results suggested that the smaller alkali cations potentially promote CO dimerization on nonaqueous electrolytes without the solvation of water molecules.[15]

Besides, the influence of cation species on the energy barriers for the *OCCO formation was also determined. The energy barrier was probed by assuming that the CO dimerization occurs between two neighboring T-sites on the Cu(100) and Pt(100) surface, where the highest energy point during C—C bond formation is defined as the transition state (TS) of the CO dimerization. As shown in Figure 2, the TS of the CO dimerization and the corresponding energy barrier were strongly affected by the alkali metal ions on Cu(100) and Pt(100) surfaces.

The Cu(100) surface showed the largest barrier of 1.16 eV when cations were absent. With the presence of cations, the energy barrier for CO dimerization is reduced dramatically to 0.33 eV with Cs^+, followed by the presence of K^+ (0.17 eV) and Na^+ (0.13 eV). In particular, the Cu(100) surface with the smallest Li^+ cations can effectively promote the rate-limiting C—C coupling step with the lowest energy barrier of less than 0.10 eV via direct cation interactions. In contrast, the energy barrier for CO dimerization was much larger on the Pt(100) surface. The Pt(100) surface shows the largest barrier of 1.12 eV for *OCCO formation without charged species. With the presence of cations, the energy barrier for CO dimerization followed the trend of $Li^+ < Na^+ < Cs^+ < K^+$ with an activation energy barrier of 0.27, 0.52, 0.77, and 0.92 eV, respectively. Intriguingly, we also noticed that the CO dimerization with lower reaction energy and energy barrier showed longer d_{C-C} on their TS, whereas those with higher reaction energy and energy barrier showed longer. The observed phenomenon is elucidated by the Hammond Postulate, which states that the structure of the TS resembles the structure of the nearest stable species.[16] The CO dimerization has a negative ΔH_{OCCO}, such as Cu(100) and Pt(100) under Li^+, and the TS has a long C—C distance (≈2.5 Å), where the TS is more like two *CO reactants. Without the cation species, the TS shows shorter C—C distances (1.6 and 1.9 Å) for endergonic CO dimerization, where the TS becomes more like *OCCO product.

2.3. Direct Stabilization Effect of Cations

Although the ΔE_{OCCO} adsorption energy could reflect the stability of the adsorption configuration. However, the linear correlation plot between ΔE_{OCCO} and ΔH_{OCCO} shows that the ΔE_{OCCO} adsorption energy only has a linear correlation with the *OCCO formation energy on the Cu(100) and Pt(100) surfaces individually (Figure S9, Supporting Information). It is believed that the limited correlation between ΔE_{OCCO} adsorption energy and $^*\Delta H_{OCCO}$ formation energy was attributed to the cation-surface and dimer-surface interactions on Cu(100) and Pt(100) surfaces. It is believed that the different surface electronic properties of Cu(100) and Pt(100) contribute to the huge difference in the ΔE_{OCCO} adsorption energy on the surfaces.

To estimate the direct stabilization effect induced by the alkali metal cations, the cation-stabilization energy (ΔE_{stab}) was determined. The ΔE_{stab} is the summation of $\Delta E_{cation-dimer}$ and $\Delta E_{cation-slab}$, and the cation–cation repulsive interaction was negligible because of the far separation. In our definition, the more negative the ΔE_{stab}, the improved cation-induced stability in the systems. As shown in **Figure 3**a,b, the ΔE_{stab} not only vary with the change of alkali metal ions but also depend on the relative ratio (cation: dimer) of the cation. For the Cu(100) surface, the ΔE_{stab} increased with the decrease in the cation size, following the $Li^+ > Na^+ > K^+ > Cs^+$ trend. While the higher relative ratio of the cation also results in more negative ΔE_{stab}. For instance, the system with three cations per CO dimer (3+) has a more negative ΔE_{stab} than the system with less cations (2+ and 1+) (Figure 3c,d). Different from the Cu(100), the ΔE_{stab} on the Pt(100) surface was much smaller than that of the Cu(100) surface. This less cation-induced stabilization on the Pt(100) surface can be attributed to the positive value of $\Delta E_{cation-slab}$ has weakened the overall stabilization effect of the cation. Also, it is worth noticing that the magnitude of $\Delta E_{cation-dimer}$ shown less surface dependency compared to the $\Delta E_{cation-slab}$ for Cu(100) and Pt(100) surfaces.

More importantly, we found that the value of $\Delta E_{cation-dimer}$ exhibits a strong correlation with the ΔH_{OCCO} on Cu(100) and Pt(100) surfaces. Especially the $\Delta E_{cation-dimer}$ has a very strong correlation with the ΔH_{OCCO} for the CO dimerization on Cu(100) surface with $R^2 = 0.972$ (Figure S10, Supporting Information). Meanwhile, this correlation is much weaker on the Pt(100) surface, with a lower R^2 of 0.797 (Figure S11, Supporting Information). Notably, ΔH_{OCCO} for Pt(100) changes slightly when varying the 1st row of alkali metal cation, especially for larger cations such as K^+ and Cs^+. This suggests that the CO dimerization process was less susceptible to the cation stabilization effects due to the over-binding effect of intermediate on Pt surfaces. Both the *CO and *OCCO are believed to be highly stable on the Pt surface, and introducing cation could not further stabilize the product *OCCO like on the Cu surface. Furthermore, as shown in **Figure 4**, there is also a strong linear correlation with $R^2 = 0.891$ between the $\Delta E_{cation-dimer}$ and the

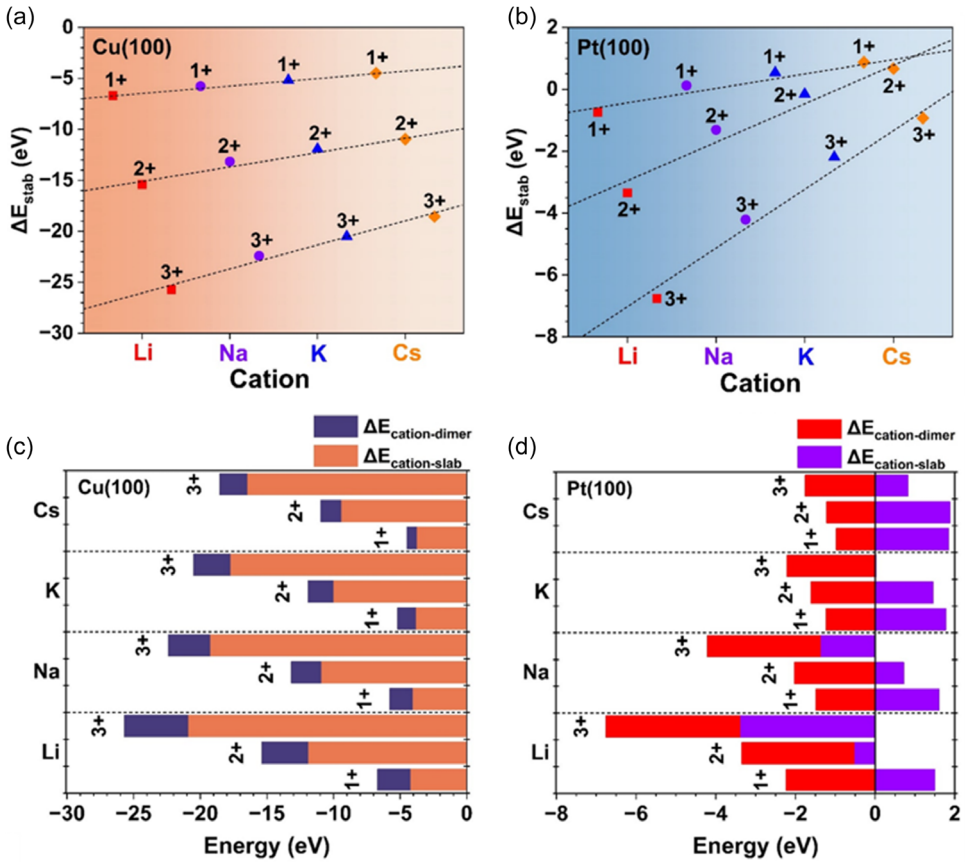

Figure 3. The calculated ΔE_{stab} for *OCCO formation for a) Cu(100) surface and b) Pt(100) surface with different alkali metal ions. The $\Delta E_{cation-dimer}$ and $\Delta E_{cation-slab}$ contributed to the ΔE_{stab} for c) Cu(100) surface and d) Pt(100) surface. The 1+, 2+, and 3+ represent relative ratios of one, two, and three cations per adsorbed *OCCO.

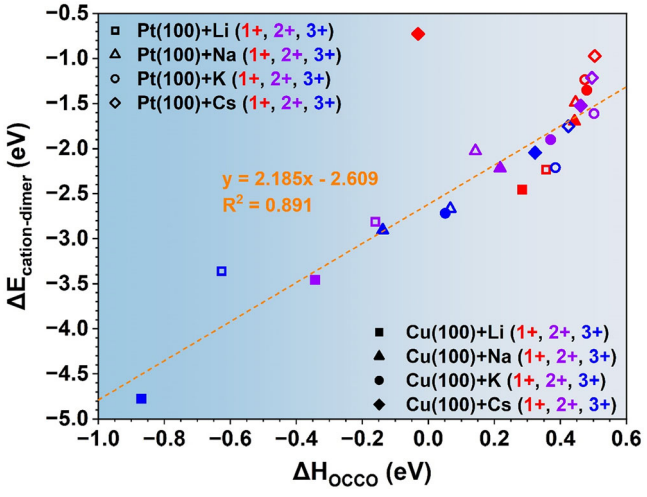

Figure 4. The linear correlation between the ΔH_{OCCO} and the $\Delta E_{cation-dimer}$ on Cu(100) and Pt(100) surface with various alkali metal ions (Li^+, Na^+, K^+ and Cs^+) and different relative ratio of the cations (1+, 2+, and 3+).

ΔH_{OCCO} when considering all the data for both Cu(100) and Pt(100) surfaces. This linear plot implies that the thermodynamic feasibility of CO dimerization is strongly connected to the direct interactions between the cation species and *OCCO, whereas the $\Delta E_{cation-dimer}$ is regarded as an indicator of the CO dimerization process. However, we notice that there is one outlier data point located at $\Delta E_{cation-dimer}$ of −0.7 eV, which is $1Cs^+$ on Cu(100). For this outlier point, no stable adsorption configuration of *OCCO was found because the weakest stabilizing ability of Cs^+ is insufficient to stabilize *OCCO with a relative ratio equal to +1. For the Pt(100) surface, most of the data points were concentrated in the region of $\Delta H_{OCCO} > 0$ eV owing to the relatively more positive value of $\Delta E_{cation-dimer}$. Meanwhile, it is also shown that the $\Delta E_{cation-dimer}$ and the corresponding ΔH_{OCCO} were regulated by both the type of alkali metal ions and the relative ratio of the cations, especially on the Cu(100) surface.

2.4. Electronic Properties of the Adsorbed OCCO with the Effect of Cations

On the other hand, previous studies have proposed that carrying a negative charge is able to stabilize the *OCCO on the metal surface. Herein, we perform Mulliken population analysis to reveal the charge distribution on the adsorbed CO dimer under different cations. **Figure 5**a,b are the Mulliken population analysis, which show that the *OCCO molecule tends to carry a

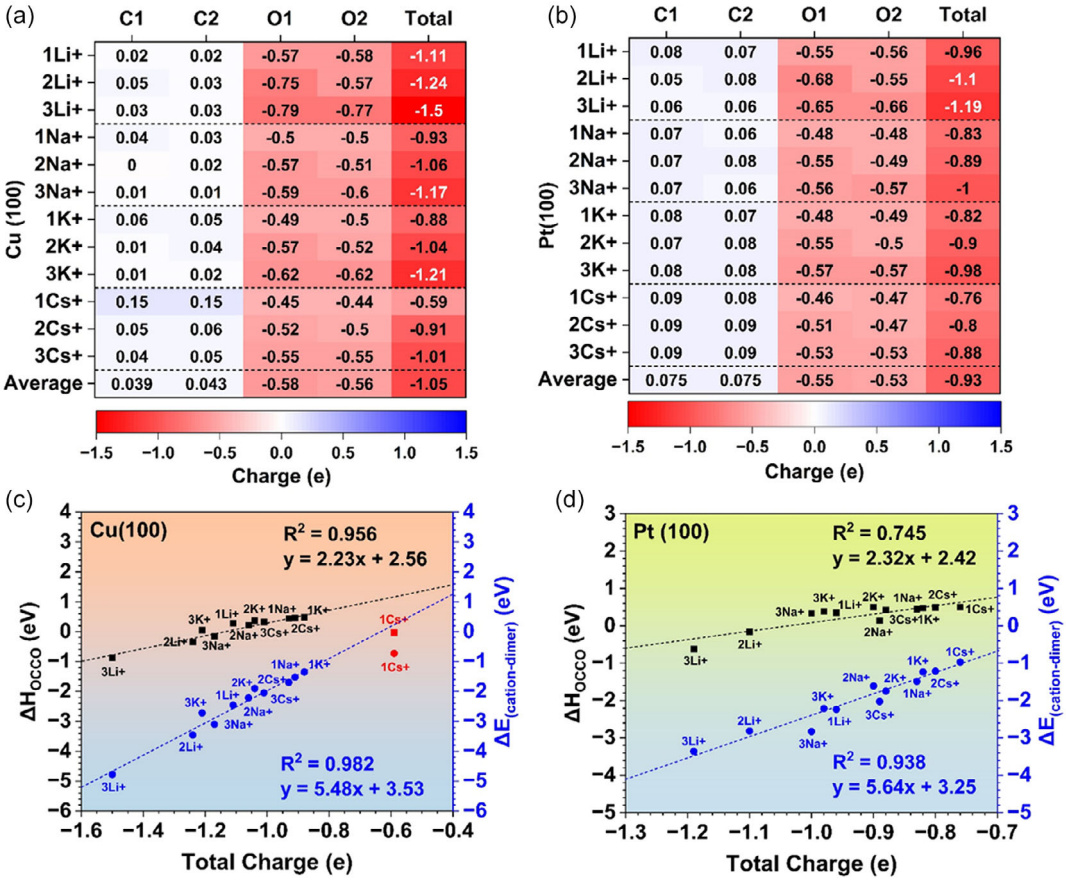

Figure 5. The Mulliken charge distribution of *OCCO molecules for a) Cu(100) surface and b) Pt(100) surface. The correlation between the total net charge on *OCCO and the stabilization effect on the c) Cu(100) surface and d) Pt(100) surface, in which the blue dots represent the stabilization effect induced by cations and black squares are the corresponding reaction energy of *OCCO formation.

negative charge on Cu(100) and Pt(100) surfaces when cation species exist. The negative charge was distributed mainly on the O atoms on the *OCCO while the C atoms attached to the metal surface with positive charges. In terms of the magnitude of the negative charge, the total charge of *OCCO molecule on the Cu(100) surface is larger (more negative) than that on the Pt(100) surface, except for the $1Cs^{+}$, where no stable *OCCO molecule was found on the Cu(100) surface. Hence a relatively smaller negative charge of −0.59 predicted for 2*CO is noted. It has demonstrated that the smaller alkali metal ions induce the negative charge accumulations on the *OCCO for both the Cu(100) and Pt(100) surfaces. Figure 5c,d demonstrates that there is also a linear correlation between the total charge and the $\Delta E_{\text{cation-dimer}}$ (and the corresponding ΔH_{OCCO}) on Cu(100) and Pt(100), supporting the idea that the carrying negative charge is the key to stabilizing the adsorbed *OCCO on metal surfaces. We also deduced that the larger magnitude of the negative charge on *OCCO is attributed to the higher charge density of the smaller cation species, which stabilize the *OCCO via the formation of the reduced form $*OCCO^{-}$.

To gain deeper insight into the electronic modification of metal surfaces, we have investigated the electronic structures of the metal surface. For the *d*-band of metal surfaces, the cation interaction and intermediates adsorption modified the electronic structure of the metal surface. Notably, the *d*-bands of metal were moved away from the Fermi level (E_F) following the adsorption intermediates (**Figure 6**a,b), in which the peak position was downshifted about 2 eV for the adsorption of *CO on Cu(100) and Pt(100). This *d*-band shifting is induced by the strong interactions between the adsorbate and the metal sites, in which the charge transfer and the surface geometry deformation are due to the *d*-band energy levels are affected by intermediate adsorptions. Notably, the formation of *OCCO brings the metal *d*-band closer to higher energy levels on Cu(100) and Pt(100) surfaces. This reveals that the adsorption of *OCCO shows less modifications to the *d*-band due to the weaker interactionse between the *OCCO and the metal sites compared to that of *CO.

Besides, different alkali ions have also introduced significant electronic structure modifications for both metal surfaces and *OCCO molecule. For the metal surfaces, the variation of the adsorption energy toward the *OCCO molecule on Cu(100) and Pt(100) surfaces should be correlated to the modification of the metal *d*-band center. According to the *d*-band center theory, the adsorption strength of an adsorbate on a transition metal surface can be determined by the *d*-band center position, which is regarded as the centroid of the metal *d*-band.[17] For transition

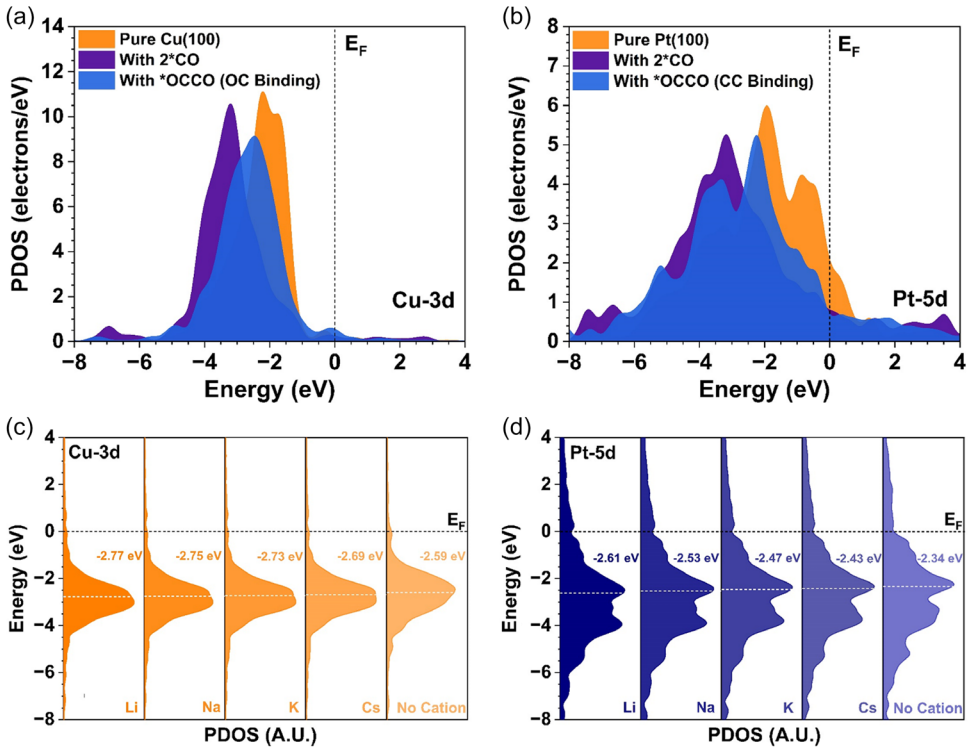

Figure 6. The shifting of the a) 3*d*-states of the Cu(100) surface and d) 5*d*-states of the Pt(100) surface due to the intermediates adsorption. c) The change of the *d*-band center position of c) Cu(100) surface and d) Pt(100) surface under the direct cations effect induced by alkali metal ions.

metals with more than half-filled *d*-states, the upshift of the metal *d*-band center toward the E_F will strengthen the adsorption because of the reduced population of antibonding states. In contrast, the downshift of the *d*-band center leads to weaker adsorbate-metal bonding owing to the increasing population of antibonding states.[18]

Figure 6c,d shows the variation of the *d*-band center. The fully-filled Cu *d*-band was located far below the E_F, and the partially-filled Pt *d*-band was pinned near the E_F to follow the Fermi–Dirac distribution. As a result, the *d*-band centers of the Pt(100) surface were much closer to the E_F than that of the Cu(100) surfaces, leading to much stronger *OCCO adsorption on the Pt surface compared to the Cu surface with low-lying *d*-band. For Cu(100) and Pt(100) surfaces, alkali cations have led to a *d*-band center downshift, indicating that the cations alleviate the *OCCO adsorption via *d*-band modification. Moreover, the upshift of the *d*-band center was observed for the larger alkali cations. For example, the stronger *OCCO adsorption on both Cu(100) and Pt(100) surfaces for Na^+, K^+, and Cs^+ ions was contributed by their upshifted *d*-band center. On the Cu(100) surface, the *d*-band center was gradually upshifted from E_V −2.77 eV to E_V −2.69 eV by changing the cation from Li^+ to Cs^+, which led to the strengthening of *OCCO adsorption from E_V −0.87 eV to E_V −1.43 eV. On the Pt(100) surface, a similar trend of *d*-band center upshift was shown. On the other hand, different from the *OCCO, the upshift of the *d*-band center led to the weaker cation species binding on Cu(100) and Pt(100) surfaces. It is believed that the 1st row alkali metal cations with zero valences are preferred to bind on the negatively charged (or electron-rich) surface. According to the calculation results of reaction energy and energy barrier, stronger *OCCO adsorption displays a larger energy cost to drive the dimerization process, and introducing smaller cations facilitates the *OCCO formation due to weaker *OCCO adsorption. However, we notice that the *d*-band center position variation is relatively small when changing the cation size. This suggests that the change in the *OCCO adsorption energy is not fully contributed by the slight variation of the *d*-band center position.

The projected partial density of the states (PDOS) analysis was performed on the metal sites and the atomic carbon on *OCCO (**Figure 7**a,b). To investigate the coupling of *p*–*d* orbitals between the carbon atom and the metal site, we examined the overlap area between the PDOS of C-2*p* and metal *d*-orbitals. The interplay between the metal valence *d*-orbital and the frontier orbitals (highest occupied molecular orbital (HOMO)/lowest occupied molecular orbital (LUMO)) of the intermediate results in the σ-region and π-region interaction. For the Cu(100) surface, both the σ-region and π-region show a significant increase in *p*–*d* overlapping by changing the cation from Cs^+ to Li^+. The *p*–*d* overlapping on the σ-region and π-region increases monotonically from 0.78 to 0.95 e^- and 0.72 to 0.89 e^-, respectively. This increase of *p*–*d* overlapping on the σ-region and π-region reflects the chemisorption interaction between the *OCCO and Cu(100) surface with directional electron transfer via the *p*–*d* orbital interaction. This significant electron transfer between the adsorbed *OCCO and Cu(100) surface was also supported by the larger Mulliken charge accumulation of the adsorbed *OCCO on Cu(100). For the Pt(100) surface, although the broad

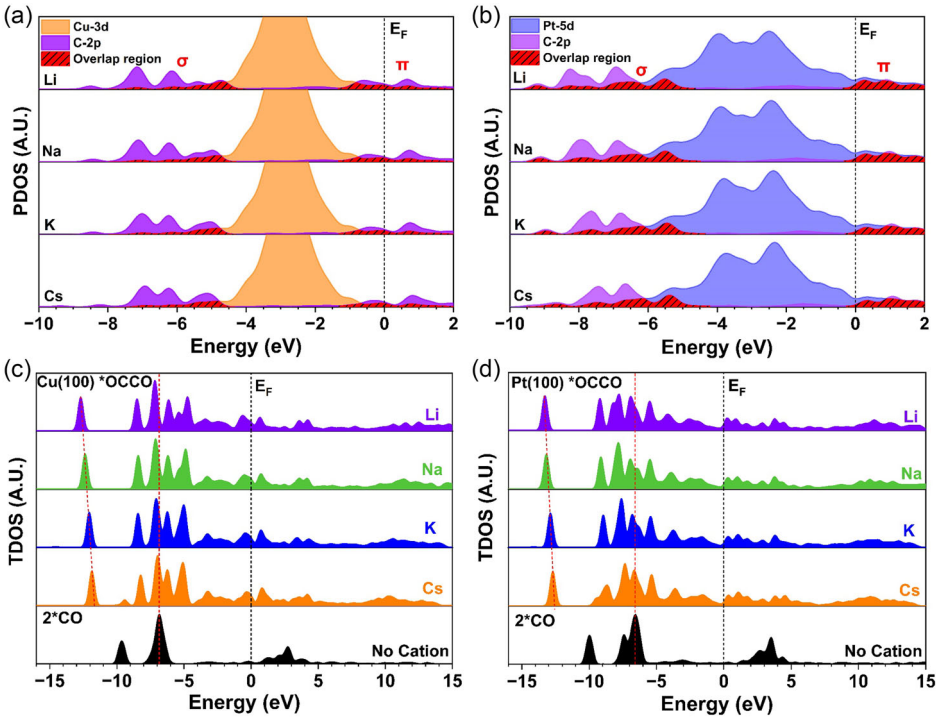

Figure 7. The projected density of the states (PDOS) and *p–d* orbital overlapping of binding metal sites and carbon atoms of *OCCO adsorbed on a) Cu(100) surface and b) Pt(100) surface. The total density of states (TDOS) of *CO and *OCCO adsorption on c) Cu(100) surface and on d) Pt(100) surface.

5*d*-orbitals result in a sizeable overlapping between the C-2*p* and Pt-5*d* orbitals compared to that of the Cu(100) surface, an opposite trend of the *p–d* overlapping on σ-region and π-region was found. The *p–d* overlapping on the σ-region decreased from 1.65 to 1.51 e^- when changing the cation from Cs^+ to Li^+, whereas the overlap on the π-region increased from 0.83 to 0.91 e^-. Hence, varying cations did not significantly affect the electron transfer between the *OCCO and Pt(100) surface, and no significant redistribution of electron density occurred. This implies that the interaction between the *OCCO and Pt(100) surface should belong to physisorption. Meanwhile, we also noticed that the empty Pt-5*d* and C-2*p* states mainly contributed to the π-region interaction between the Pt(100) and carbon atom. This revealed that for the Pt(100) surface, the π-region interaction is mainly ionic/electrostatic interactions because of the partially filled π-region. On the other hand, the variation of cations has also induced a significant change in the C-2*p* orbitals population in energy level around E_V−5.0 to E_V−7.5 eV (E_V denotes 0 eV), especially for the Cu(100) surface. Changing the alkali metal ions from Cs^+ to Li^+ increased the splitting of 2*p* peaks around E_V−6.5 eV, suggesting the stronger C—C bond formation under smaller alkali ions. This is well matched with the bond length reduction of the *OCCO in Table 1 and Figure 1, where the C—C bond length decreases from 1.610 to 1.482 Å on the Cu(100) surface and from 1.573 to 1.519 Å on the Pt(100) surface.

Figure 7c,d shows the total density of states (TDOS) of the *CO and *OCCO on Cu(100) and Pt(100) surfaces under different alkali metal ions. Compared with the TDOS of 2*CO on the metal surface, which only displays a singlet peak at around E_V−7.0 eV, the C—C bond formation on *OCCO was indicated by the multiple patterns, supporting the splitting of C 2p peaks in PDOS (Figure 7a,b) is associated with the C—C coupling. Meanwhile, the Cu(100) surface displays much smoother 2*CO to *OCCO conversions than the Pt(100) surface. It is also found that the TDOS near E_F region is lower for the 2*CO, in which the HOMO)and LUMO were separated by a wide energy gap, indicating that there was no significant electron transfer and the adsorbed *CO was inactivated before C—C coupling. In contrast, the *OCCO displays higher TDOS on the near E_F region, especially for the Cu(100) surface, suggesting that the formation of *OCCO was promoted via the effective electron delocalization on the Cu(100) surface. We also noticed that the peaks of the TDOS of *OCCO gradually move to the lower energy side when the alkali metal ions vary from Cs^+ to Li^+. The larger $\Delta E_{cation-dimer}$ and smaller ΔH_{OCCO} for smaller alkali metal ions are consistent with this downward peak shift in the TDOS. This suggests that the smaller cations with higher positive charge density stabilize the electrons on the *OCCO via electrostatic cation–dimer interaction.

3. Perspective to Other C—C Couplings

According to previous studies, the C—C coupling reaction pathways mainly included the coupling between *CO and *CO/*CHO/*COH species.[19] For alternative *CO—*CHO/*COH coupling pathways, the *CO needed to be hydrogenated into *CHO or *COH before undergoing C—C bond formation, in

which the *CO hydrogenation dominates the metal surface at high potential.[20] Although the presence of water and the solvation effects can reduce the energy barrier for *CO hydrogenation, the CO hydrogenation reaction is energetically uphill on metal surfaces with the solvation model.[21] This suggests that the hydrogenation of *CO is also a key elementary step for the C_{2+} pathway. Meanwhile, the calculations also found that the formation of *COH is unfavorable on the Cu(100) surface.[22] Hence, the coupling between *COH and *CO was rarely considered for CO_2RR on Cu(100) surfaces. For the coupling via *CHO intermediate, previous research has shown that the *CO*—CHO coupling is more favorable than the *CO-*CO dimerization on Cu(100) only in the vacuum condition, whereas the CO dimerization reaction has a much lower reaction energy barrier in the explicit solvent model.[23]

On the other hand, the dimerization between two adsorbed *CO takes place on the Cu surface at low potential.[24] Although the experiment conducts the CO_2RR electrocatalyst at high potential, the future industrial CO_2RR electrocatalyst design always aims to reduce the operation voltage to save energy consumption and cost. Meanwhile, the CO_2 has been selectively reduced to ethylene at low overpotential under alkaline conditions on the Cu(100) surface, while the computational study has also found that the CO dimerization reaction has a much lower reaction energy barrier in the explicit solvent model.[25] These results suggest that the CO dimerization proceeds before the formation of *CHO with the presence of solvent on the Cu(100) surface. Based on that, our work chose * CO—*CO dimerization as the main focus to investigate the direct cation effects in the C—C coupling process. To further discuss the different C—C coupling pathways, we have also performed some comparisons based on our results and other research works regarding the C—C coupling.

As shown in Table S2, Supporting Information, the Cu(100) surface could not strongly adsorb the *CHO intermediate on the Cu(100) surface without the presence of cation owing to the positive *CHO adsorption energy of 0.51 eV. The cation effects of Li^+, Na^+, and Cs^+ strengthen the adsorption of *CHO on the Cu(100) surface of ≈0.5 eV, but the adsorption of *CHO is still much weaker than other key intermediates (Figure S12, Supporting Information). The weak *CHO adsorption strength may indicate that the *CHO has difficulty retaining high coverage compared to the *CO, leading to the coupling between *CO and *CHO rarely occurring on the Cu(100) surface. Similarly, the adsorption strength of *OCCO is stronger than that of *OCCHO on the Cu(100) surface with the effect of cations, suggesting that the *OCCO is more stable than the *OCCHO intermediate under the cation effects. On the other hand, for the compassion of the C—C coupling energy barrier, the *CO hydrogenation has a lower energy barrier than the CO dimerization without the introduction of cations. However, with the introduction of cations, the energy barrier for direct CO dimerization has significantly dropped, whereas the energy barrier for *CHO formation has only changed slightly (Figure S13, Supporting Information). As a result, the energy barriers for CO dimerization were much lower than that of the *CHO formation on the Cu(100) surface. Combining our work with previous studies demonstrated that CO dimerization is much more favored than the coupling between *CHO and *CO on the Cu(100) surface with the cation effects. Furthermore, previous calculations have concluded that the cation effects on promoting CO dimerization are due to the larger stabilization of the intermediate containing C—C bond when compared to the C_1 intermediate on the metal surface, suggesting that the direct cation effects could play a similar role on other C—C coupling routes.[11] Based on that, the calculation results of this work can be used as the initiation point for future study of the coupling among *CHO/*COH/*CO species.

4. Conclusion

In summary, the direct cation effects on the CO dimerization process on Cu(100) and Pt(100) surfaces were investigated through the calculation of adsorption energy, activation energy barrier, reaction energy, stabilization energy, and electronic properties such as charge distribution and PDOS using DFT. The calculation results demonstrated that the presence of alkali metal ions significantly promotes *OCCO formation via direct cation stabilization. The activation energy barrier and reaction energy of the *OCCO formation showed that the smaller Li^+ cation reduces the energy cost for CO dimerization more obviously. In particular, a strong linear correlation between the cation–dimer stabilization and reaction energy was found in the presence of alkali metal ions. Additionally, the population analysis also demonstrated that the stabilization effect induced by cation was related to the negative charge accumulation on adsorbed *OCCO, in which the *OCCO formation on Cu(100) surface with smaller alkali metal ions is beneficial from the larger magnitude of the negative charge. Lastly, the electronic structures of the Cu(100) and Pt(100) surfaces were modified by the adsorption of intermediates as well as the cation effects, which showed that the forming of new C—C bonds and the introduction of cations during CO dimerization alter the *d*-band of the metal surfaces. Meanwhile, the favorable *OCCO formation on Cu(100) with a smaller Li^+ cation was also indicated by the PDOS profile. More importantly, this work will provide fundamental insight into the intrinsic effects induced directly by cations for the CO dimerization process and will open great opportunities for synthesizing C_2 products via CO_2RR.

5. Experimental Section

Calculation Setup: In this work, DFT calculations were performed in the Cambridge Serial Total Energy Package (CASTEP).[26] The Perdew–Burke–Ernzerhof generalized gradient approximation method was used to describe the exchange-correlation energy for all the model calculations.[27] Moreover, the Broyden–Fletcher–Goldfarb–Shanno algorithm was adopted as the optimizer, and the ultrasoft pseudopotential scheme was applied for the geometry optimization.[28] Pt(100) and Cu(100) metal slabs with a 4 × 4 supercell and five atomic layers were used to simulate the adsorption behaviors. The vacuum thickness along the *z*-axis perpendicular to the surface was set as 20 Å to prevent spurious interactions between the repeated slabs. In addition, the plane-wave cutoff energies were set as 380 eV for the Pt(100) adsorption model and 440 eV for the Cu(100) adsorption model, while the k-point grid parameter was set with coarse quality. Convergence criteria for the single point energy calculation and the geometry optimizations were defined as follows: the SCF tolerance is 1.0×10^{-5} eV atom^{-1}, the Hellmann–Feynman force per atom is 0.1 eV Å^{-1}, the Maximum stress is 0.2 GPa; and the Maximum displacement is 0.005 Å. For the CO dimerization process, the bridge

location between two neighboring top-sites (T-sites) on the Pt(100) and Cu(100) surface was selected as the adsorption sites of the *OCCO molecule. The adsorption energy (ΔE_{OCCO}) of the *OCCO on these sites can be calculated using the following equation

$$\Delta E_{OCCO} = E_{slab/OCCO} - E_{slab} - E_{OCCO} \quad (1)$$

where the $E_{slab/OCCO}$ is the total energy of the metal slab binding with *OCCO intermediate. The E_{slab} and E_{OCCO} are the energy of the metal slab and isolated OCCO, respectively.

On the other hand, we define the total cationic stabilization effects as the cation-stabilization energy (ΔE_{stab}), calculated as the overall interaction energy ($\Delta E_{interaction}$) in the system (E_{system}) minus the adsorption energy of *OCCO intermediate

$$\Delta E_{interaction} = E_{system} - (E_{slab} + E_{OCCO} + E_{cation}) \quad (2)$$

$$\Delta E_{stab} = \Delta E_{interaction} - \Delta E_{OCCO} \quad (3)$$

$$\Delta E_{stab} = \Delta E_{cation-slab} + \Delta E_{cation-dimer} \quad (4)$$

The $\Delta E_{cation-slab}$, $\Delta E_{cation-dimer}$, and E_{cation} are the cation-slab interaction energy, cation–dimer stabilization energy, and cation species energy, respectively.

Supporting Information

Supporting Information is available from the Wiley Online Library or from the author.

Acknowledgements

The authors gratefully acknowledge the support from the National Key R&D Program of China (grant no. 2021YFA1501101), Research Grant Council of Hong Kong (grant no. 15304023), National Natural Science Foundation of China/Research Grant Council of Hong Kong Joint Research Scheme (grant no. N_PolyU502/21), National Natural Science Foundation of China/Research Grants Council of Hong Kong Collaborative Research Scheme (grant no. CRS_PolyU504/22), the funding for Projects of Strategic Importance of The Hong Kong Polytechnic University (Project Code: 1-ZE2V), Shenzhen Fundamental Research Scheme-General Program (grant no. JCYJ20220531090807017), Natural Science Foundation of Guangdong Province (grant no. 2023A1515012219), and Departmental General Research Fund (Project Code: ZVUL) from The Hong Kong Polytechnic University. The authors also thank the support from Research Centre for Carbon-Strategic Catalysis (RC-CSC), Research Institute for Smart Energy (RISE), and Research Institute for Intelligent Wearable Systems (RI-IWEAR) of the Hong Kong Polytechnic University.

Conflict of Interest

The authors declare no conflict of interest.

Data Availability Statement

The data that support the findings of this study are available from the corresponding author upon reasonable request.

Keywords

alkali metal cations, cation effect, CO dimerization, CO_2 reduction reaction, stabilization effects

Received: April 8, 2024
Revised: April 24, 2024
Published online: May 12, 2024

[1] a) J. Du, P. Zhang, H. Liu, *Chem* **2021**, *16*, 588; b) S. Zaman, S. Chen, *J. Catal.* **2023**, *421*, 221.
[2] a) D. D. Zhu, J. L. Liu, S. Z. Qiao, *Adv. Mater.* **2016**, *28*, 3423; b) L. Zhang, Z.-J. Zhao, J. Gong, *Angew. Chem. Int. Ed.* **2017**, *56*, 11326; c) K. Li, B. Peng, T. Peng, *ACS Catal.* **2016**, *6*, 7485.
[3] a) S. Nitopi, E. Bertheussen, S. B. Scott, X. Liu, A. K. Engstfeld, S. Horch, B. Seger, I. E. L. Stephens, K. Chan, C. Hahn, J. K. Nørskov, T. F. Jaramillo, I. Chorkendorff, *Chem. Rev.* **2019**, *119*, 7610; b) M. Sun, H. H. Wong, T. Wu, A. W. Dougherty, B. Huang, *Adv. Energy Mater.* **2022**, *12*, 2103781; c) B. Xiong, Y. Yang, J. Liu, Z. Hua, Y. Yang, *Fuel Process. Technol.* **2022**, *233*, 107315; d) H. Ait Ahsaine, A. BaQais, *Green Chem. Lett. Rev.* **2023**, *16*, 2160215.
[4] a) T. Liu, J. Sang, H. Li, P. Wei, Y. Zang, G. Wang, *Battery Energy* **2022**, *1*, 20220012; b) T. K. Todorova, M. W. Schreiber, M. Fontecave, *ACS Catal.* **2020**, *10*, 1754; c) E. Ruiz-López, J. Gandara-Loe, F. Baena-Moreno, T. R. Reina, J. A. Odriozola, *Renew. Sustainable Energy Rev.* **2022**, *161*, 112329.
[5] a) F. Calle-Vallejo, M. T. M. Koper, *Angew. Chem. Int. Ed.* **2013**, *52*, 7282; b) A. J. Garza, A. T. Bell, M. Head-Gordon, *ACS Catal.* **2018**, *8*, 1490.
[6] J. Mato, D. Poole, M. S. Gordon, *J. Phys. Chem. A* **2020**, *124*, 8209.
[7] a) J. Resasco, L. D. Chen, E. Clark, C. Tsai, C. Hahn, T. F. Jaramillo, K. Chan, A. T. Bell, *J. Am. Chem. Soc.* **2017**, *139*, 11277; b) R. B. Sandberg, J. H. Montoya, K. Chan, J. K. Nørskov, *Surf. Sci.* **2016**, *654*, 56.
[8] J.-B. Le, A. Chen, Y. Kuang, J. Cheng, *Natl. Sci. Rev.* **2023**, *10*, nwad105.
[9] A. Bagger, L. Arnarson, M. H. Hansen, E. Spohr, J. Rossmeisl, *J. Am. Chem. Soc.* **2019**, *141*, 1506.
[10] J. Li, X. Li, C. M. Gunathunge, M. M. Waegele, *Proc. Natl. Acad. Sci. U.S.A.* **2019**, *116*, 9220.
[11] E. Pérez-Gallent, G. Marcandalli, M. C. Figueiredo, F. Calle-Vallejo, M. T. M. Koper, *J. Am. Chem. Soc.* **2017**, *139*, 16412.
[12] a) J. Hussain, H. Jónsson, E. Skúlason, *ACS Catal.* **2018**, *8*, 5240; b) M. Umeda, Y. Niitsuma, T. Horikawa, S. Matsuda, M. Osawa, *ACS Appl. Energy Mater.* **2020**, *3*, 1119.
[13] M. M. Sartin, Z. Yu, W. Chen, F. He, Z. Sun, Y.-X. Chen, W. Huang, *J. Phys. Chem. C* **2018**, *122*, 26489.
[14] V. J. Ovalle, Y.-S. Hsu, N. Agrawal, M. J. Janik, M. M. Waegele, *Nat. Catal.* **2022**, *5*, 624.
[15] T. Mairegger, H. Li, C. Grießer, D. Winkler, J. Filser, N. G. Hörmann, K. Reuter, J. Kunze-Liebhäuser, *ACS Catal.* **2023**, *13*, 5780.
[16] N. M. Donahue, *J. Phys. Chem. A* **2001**, *105*, 1489.
[17] a) B. Hammer, J. K. Nørskov, *Surf. Sci.* **1995**, *343*, 211; b) A. Ruban, B. Hammer, P. Stoltze, H. L. Skriver, J. K. Nørskov, *J. Mol. Catal. A: Chem.* **1997**, *115*, 421.
[18] a) A. Nilsson, L. G. M. Pettersson, B. Hammer, T. Bligaard, C. H. Christensen, J. K. Nørskov, *Catal. Lett.* **2005**, *100*, 111; b) J. K. Nørskov, F. Abild-Pedersen, F. Studt, T. Bligaard, *Proc. Natl. Acad. Sci. U.S.A.* **2011**, *108*, 937.
[19] a) K. P. Kuhl, E. R. Cave, D. N. Abram, T. F. Jaramillo, *Energy Environ. Sci.* **2012**, *5*, 7050; b) X. Liu, P. Schlexer, J. Xiao, Y. Ji, L. Wang, R. B. Sandberg, M. Tang, K. S. Brown, H. Peng, S. Ringe, C. Hahn, T. F. Jaramillo, J. K. Nørskov, K. Chan, *Nat. Commun.* **2019**, *10*, 32; c) K. Yao, J. Li, H. Wang, R. Lu, X. Yang, M. Luo, N. Wang, Z. Wang, C. Liu, T. Jing, S. Chen, E. Cortés, S. A. Maier, S. Zhang, T. Li, Y. Yu, Y. Liu, X. Kang, H. Liang, *J. Am. Chem. Soc.*

2022, *144*, 14005; d) A. A. Peterson, F. Abild-Pedersen, F. Studt, J. Rossmeisl, J. K. Nørskov, *Energy Environ. Sci.* **2010**, *3*, 1311.
[20] J. D. Goodpaster, A. T. Bell, M. Head-Gordon, *J. Phys. Chem. Lett.* **2016**, *7*, 1471.
[21] K. Nagita, K. Kamiya, S. Nakanishi, Y. Hamamoto, Y. Morikawa, *J. Phys. Chem. C* **2024**, *128*, 4607.
[22] L. Ou, W. Long, Y. Chen, J. Jin, *RSC Adv.* **2015**, *5*, 96281.
[23] J. Santatiwongchai, K. Faungnawakij, P. Hirunsit, *ACS Catal.* **2021**, *11*, 9688.
[24] J. H. Montoya, C. Shi, K. Chan, J. K. Nørskov, *J. Phys. Chem. Lett.* **2015**, *6*, 2032.
[25] K. J. P. Schouten, Z. Qin, E. Pérez Gallent, M. T. M. Koper, *J. Am. Chem. Soc.* **2012**, *134*, 9864.
[26] M. D. Segall, J. D. L. Philip, M. J. Probert, C. J. Pickard, P. J. Hasnip, S. J. Clark, M. C. Payne, *J. Phys.: Condens. Matter* **2002**, *14*, 2717.
[27] a) J. P. Perdew, K. Burke, M. Ernzerhof, *Phys. Rev. Lett.* **1996**, *77*, 3865; b) J. P. Perdew, J. A. Chevary, S. H. Vosko, K. A. Jackson, M. R. Pederson, D. J. Singh, C. Fiolhais, *Phys. Rev. B* **1992**, *46*, 6671.
[28] a) J. D. Head, M. C. Zerner, *Chem. Phys. Lett.* **1985**, *122*, 264; b) D. Vanderbilt, *Phys. Rev. B* **1990**, *41*, 7892.